

Structure of a Water Monolayer on the Anatase TiO₂(101) Surface

Christopher E. Patrick and Feliciano Giustino*

Department of Materials, University of Oxford, Parks Road, Oxford OX1 3PH, United Kingdom

(Received 25 March 2014; published 2 July 2014)

Titanium dioxide (TiO₂) plays a central role in the study of artificial photosynthesis, owing to its ability to perform photocatalytic water splitting. Despite over four decades of intense research efforts in this area, there is still some debate over the nature of the first water monolayer on the technologically relevant anatase TiO₂(101) surface. In this work, we use first-principles calculations to reverse engineer the experimental high-resolution x-ray photoelectron spectra measured for this surface by Walle *et al.* [J. Phys. Chem. C 115, 9545 (2011)] and find evidence supporting the existence of a mix of dissociated and molecular water in the first monolayer. Using both semilocal and hybrid functional calculations, we revise the current understanding of the adsorption energetics by showing that the energetic cost of water dissociation is reduced via the formation of a hydrogen-bonded hydroxyl-water complex. We also show that such a complex can provide an explanation of an unusual superstructure observed in high-resolution scanning tunneling microscopy experiments.

DOI: 10.1103/PhysRevApplied.2.014001

I. INTRODUCTION

The realization of artificial photosynthesis hinges on our ability to engineer materials and devices which can effectively convert solar energy into fuels [1]. Since the discovery of photocatalytic water splitting more than four decades ago [2], titanium dioxide (TiO₂) has been a lead contender in this field and has found applications in a variety of cutting-edge research areas [3–5]. As water is ubiquitous in all these applications, it is not surprising that numerous studies have been devoted to understanding the physics of the interface between TiO₂ and H₂O, particularly the rutile (110) surface [6–11]. However, in the context of nanotechnology the anatase (101) surface is even more interesting, since this is the most common surface in nanostructured TiO₂ [12–14].

A fundamental question in this area is whether H₂O molecules adsorbed on the anatase surface are intact (molecular adsorption) or dissociated into a hydroxyl group and a proton (dissociative adsorption). Until very recently, experimental and theoretical studies consistently promoted the notion that only molecular adsorption occurs on the pristine anatase (101) surface. In fact, the density-functional theory (DFT) study of Ref. [15] finds molecular adsorption to be energetically favorable over dissociation by 0.44 and 0.28 eV per H₂O molecule (at low and monolayer coverage, respectively). A few years later, the authors of Ref. [16] concluded in favor of the molecular adsorption scenario, based on their analysis of x-ray photoelectron spectroscopy (XPS) and temperature-programmed desorption (TPD) experiments. Furthermore, apart from a couple of exceptions [17,18], most

computational studies continue to find molecular adsorption to be energetically favorable [19].

More recently, scanning tunneling microscopy (STM) experiments combined with DFT calculations identified molecular water on the anatase surface at very low coverage [20]. The interpretation of STM images for higher coverages proved more challenging due to the appearance of an unexpected 2 × 2 superstructure. Then, in contrast with the prevailing view of molecular adsorption of water on anatase, the authors of a recent high-resolution XPS study [21] reported the presence of OH groups at the surface and challenged the accepted model of the interface. From an analysis of the XPS spectral intensities, the authors of Ref. [21] proposed that, at monolayer coverage, (23 ± 5)% of the water molecules dissociate into a hydroxyl and a proton.

In this work, we test the proposal of dissociative water adsorption of Ref. [21] by using first-principles calculations. Our approach consists of calculating the O 1s core-level spectra of interface models where water is adsorbed either molecularly or dissociatively and comparing our *ab initio* spectra to the experimental data of Ref. [21]. The present analysis is motivated by the very high accuracy (< 0.2 eV) that can now be achieved in DFT calculations of core-electron binding energies, as demonstrated by recent work [22–24].

As we show below, the comparison between our calculated spectra and experiment provides evidence for the presence of dissociated water in the experiments of Ref. [21] on anatase TiO₂(101) at monolayer (ML) coverage. This finding prompts us to reexamine the factual evidence underlying the molecular model of the TiO₂:H₂O interface [15,16,19,20], namely, the unfavorable energetics calculated for dissociative adsorption and the measured STM images. We find that the energetics of H₂O

*feliciano.giustino@materials.ox.ac.uk

dissociation on anatase is altered when two water molecules are adsorbed on adjacent sites. In these conditions, the energetic cost of dissociation is compensated by the energy gain due to the formation of the H-bonded complex $\text{HO} \cdots \text{H}_2\text{O}$, and dissociative adsorption becomes possible. This H-bonded complex also leads to a 2×2 superstructure like that observed in the STM images of Ref. [20].

II. METHODOLOGY

Calculations are performed within the generalized-gradient approximation to DFT of Perdew, Burke, and Ernzerhof (the PBE functional [25]), employing pseudopotentials, plane-wave basis sets, and periodic boundary conditions [14,22,24,26–28] as implemented in the QUANTUM ESPRESSO distribution [29] (technical details are given in Appendix A 1). For the sake of accuracy, adsorption energy calculations are also performed with the PBE0 hybrid functional [30]. Core-level shifts are calculated as differences in DFT total energies between systems containing a core hole, as obtained by replacing the pseudopotential of a given oxygen atom by one containing a hole in the $1s$ level [31,32]. In order to minimize the unphysical interaction of charged replicas [24,27], we use model systems containing up to 432 atoms and 3200 electrons. As in experiment, we can determine core-electron binding energies only modulo a constant, which here we choose such that the calculated bulk $\text{O } 1s$ peak is aligned to the experimental spectra.

The photoelectron spectrum $I(E)$ is determined by using the expression $I(E) = \sum_i \exp(-z_i/\lambda) \delta(E - E_i)$. Here E_i is the $\text{O } 1s$ binding energy of the atom i at a distance z_i below the surface, δ is the Dirac δ function, and the exponential accounts for the finite escape depth λ of the photoelectrons [33]. In the sum, we explicitly include the contributions of the adsorbates and those of the six topmost TiO_2 layers of the slab. In order to also describe the contribution of bulk TiO_2 far from the surface, we add the contributions from an infinite number of “virtual” atoms, whose positions are determined by the bulk anatase lattice. The $\text{O } 1s$ binding energy of virtual atoms was set to the average value taken over the central four TiO_2 layers of our slab model. The photoelectron escape depth was set to $\lambda = 3.5 \text{ \AA}$, consistent with the range 2–12 \AA determined from the universal curve [33] for kinetic energies of approximately 80 eV [21]. Different values of λ change the relative strengths of the bulk and adsorbate contributions to the spectrum but preserve the adsorbate features (see Appendix A 2). The Dirac δ functions are replaced by Gaussians in order to account for vibrational broadening, core-hole lifetimes, and instrumental resolution. We evaluated the vibrational broadening by using importance-sampling Monte Carlo calculations as in Ref. [34]. Quantum zero-point motion is found to induce a significant broadening, with a FWHM of approximately 1 eV. Accordingly, we set the FWHM in

the Gaussian broadening to 1.2 eV. This choice should be representative of all the aforementioned broadening effects. For the purpose of resolving individual contributions, in the following figures we also show spectra obtained by using a very small artificial broadening of 0.1 eV. In all the figures, a linear background is subtracted from the experimental data.

III. RESULTS AND DISCUSSION

Figure 1 shows a ball-and-stick representation of the clean anatase $\text{TiO}_2(101)$ surface and its corresponding $\text{O } 1s$ core-level spectrum. Most of the oxygen atoms in the substrate, including the twofold-coordinated O atoms at the surface, contribute to a single peak at 530.17 eV, with a very small spread of 0.05 eV (right peak of the gray shaded area). Two important exceptions appear as satellites at 530.42 and 530.76 eV, indicated by arrows. These satellites arise from the structural relaxation taking place at the surface [14]. The fivefold-coordinated Ti atoms at the surface relax towards the substrate, causing a 0.1- \AA contraction of the Ti—O bond formed with a nearest-neighbor O atom underneath (indicated in blue). This contraction is responsible for an increase in the $\text{O } 1s$ binding energy by 0.59 eV with respect to the bulk (blue arrow). Similarly, the surface relaxation also causes a distortion in the second O layer (marked in green), raising these atoms by 0.34 \AA out of their ideal planar bonding with the three Ti neighbors. This distortion is responsible for an increase in binding energy by 0.25 eV (green arrow). Figure 1 shows that our calculations are in very good agreement with the experimental spectrum reported in Ref. [21] for the clean anatase surface (light blue circles), with the structural relaxation effects accounting for the slight asymmetry in the experimental line shape.

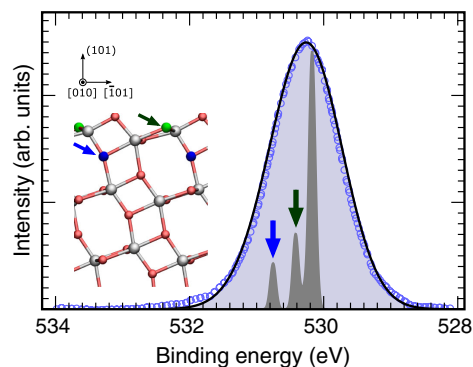


FIG. 1. Calculated $\text{O } 1s$ core-level spectrum of the clean anatase $\text{TiO}_2(101)$ surface, compared to experiment [21] (blue circles). The black line and dark shaded area correspond to a Gaussian broadening of 1.2 and 0.1 eV, respectively. The inset shows a ball-and-stick model of the anatase (101) surface, with O atoms in red and Ti atoms in white. The O atoms represented in green and blue give rise to the two satellites indicated by the arrows.

Next we investigate the core-level spectra in the presence of water at low coverage. We consider both molecular and dissociative adsorption, as shown by the atomistic models in Fig. 2. In molecular adsorption, the H_2O molecule forms a dative bond with a fivefold-coordinated Ti atom at the surface [bond length 2.32 Å, Fig. 2(a)]. In dissociative adsorption, the OH group bonds covalently to a fivefold Ti atom (bond length 1.82 Å), and the proton bonds to a twofold-coordinated O atom, thereby yielding an additional hydroxyl group [Fig. 2(b)]. In Appendix A 3 we explore models differing in the separation between the two OH groups, but here we focus on the model shown in Fig. 2(b) previously described as the “intrapair configuration” [15] or “pseudodissociated water” [21].

Considering molecular adsorption first [Fig. 2(a)], we observe that the calculated spectrum exhibits a new feature at 534.03 eV arising from the O atom of the water molecule. At the same time, in the energy range 528–532 eV the spectrum is identical to that of the clean surface (Fig. 1). This observation is explained by noting that the dative H_2O —Ti bond does not induce any significant distortion in the underlying substrate. In the case of dissociative adsorption, the spectrum exhibits two new contributions at 531.34 and 531.93 eV, arising from the inequivalent OH groups marked by the green and blue arrows. Other configurations (Appendix A 3) yield essentially identical results.

In Figs. 2(a) and 2(b), we compare our calculated spectra at low coverage (0.25 ML) with the XPS data of Ref. [21] corresponding to a coverage of 0.1 ML. The experimental spectrum is closely reproduced by our calculation in Fig. 2(b) but not by the calculation in Fig. 2(a). This observation leads us to support the proposal of Ref. [21] of predominantly dissociative adsorption over molecular adsorption at low coverage in their experiments.

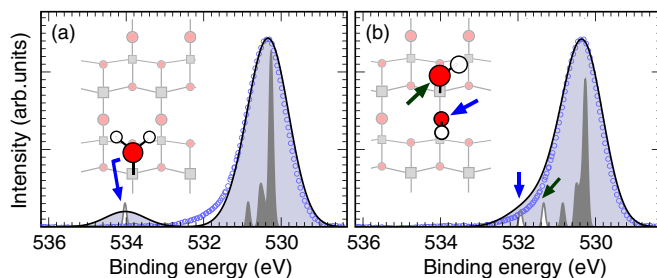


FIG. 2. Calculated O $1s$ core-level spectra for the $\text{TiO}_2:\text{H}_2\text{O}$ interface at low coverage for molecular (a) and dissociative (b) adsorption, compared with the experimental O $1s$ spectrum at 0.1-ML coverage (blue circles, spectrum at 300 K in Fig. 3 of Ref. [21]). Black and gray lines correspond to a Gaussian broadening of 1.2 and 0.1 eV, respectively. The insets show ball-and-stick models viewed from above with squares and circles representing Ti and O, respectively. The arrows identify O $1s$ shifts of particular atoms. Dark shaded areas indicate the contributions from the TiO_2 substrate.

Having addressed the clean surface and water at low coverage, we now consider the case of a full water monolayer. Following the proposal of Ref. [21], we investigate two interface structures: one comprised only of water molecules and another one where 25% of the molecules underwent dissociation. Figure 3 shows the lowest-energy structure among the four inequivalent models allowed by our choice of surface supercell.

The spectrum calculated for the partially dissociated monolayer (black line in Fig. 3) exhibits two key differences with respect to the undissociated monolayer (red line). The first is a shoulder in the substrate peak around 532 eV. This effect arises from the presence of hydroxyl groups, as discussed in relation to Fig. 2. The second is a broadening and a redshift of the water peak around 534 eV. This feature is explained as follows. The OH group obtained from water dissociation interacts strongly with a neighboring H_2O molecule. This interaction leads to the formation of a $\text{HO}\cdots\text{H}_2\text{O}$ complex carrying a distinct spectral fingerprint (gray shaded curve in Fig. 3). In fact, the hydrogen bond between OH and H_2O (length 1.71 Å) reduces the O $1s$ binding energy on the coordinated H_2O molecule by 0.64 eV compared to the other water molecules. The reduction of core-level binding energies by H bonds is a well-documented effect [22,35]. The broadening and redshift observed in Fig. 3 result therefore from the presence of two different species on the surface: molecular H_2O and the $\text{HO}\cdots\text{H}_2\text{O}$ complex.

When we compare our calculations with the XPS data of Ref. [21] at monolayer coverage (Fig. 3), we find that the spectrum calculated for the partially dissociated water monolayer is in excellent agreement with experiment, in contrast to that calculated for undissociated water. This comparison supports the proposal of Ref. [21] of

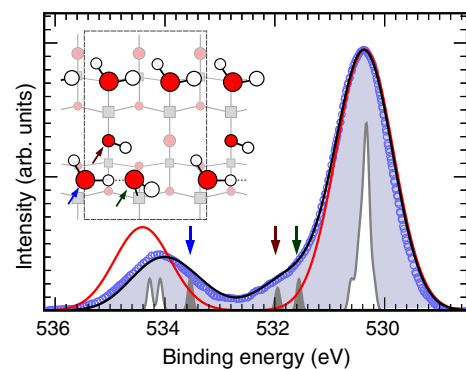


FIG. 3. Calculated O $1s$ core-level spectra for the $\text{TiO}_2:\text{H}_2\text{O}$ interface at monolayer coverage, for molecular (red curve) and partial dissociative adsorption (black and gray curves), with the experimental O $1s$ spectrum (blue circles, spectrum at 230 K in Fig. 3 of Ref. [21]). The inset shows a ball-and-stick model of the partially dissociated monolayer viewed from above. The arrows and dark shaded area identify the O $1s$ signature of the $\text{HO}\cdots\text{H}_2\text{O}$ complex.

dissociative water adsorption on the anatase $\text{TiO}_2(101)$ surface in their experiments.

This result appears to contradict the commonly accepted molecular model of the $\text{TiO}_2:\text{H}_2\text{O}$ interface [15,16,19,20]. While we cannot rule out the possibility that water dissociation in the experiments of Ref. [21] may be induced by the x-ray irradiation [36], our present finding requires us to critically reexamine previous evidence for molecular adsorption. In this spirit, we first consider the calculation of the energetics of water adsorption.

Careful test calculations indicate that the adsorption energy is rather sensitive to the thickness of the TiO_2 model slab and the sampling of the surface Brillouin zone (Appendix A 4). In the case of the undissociated water monolayer, our converged adsorption energy (obtained by using eight TiO_2 layers and a 2×2 surface Brillouin zone mesh) is 0.64 eV per water molecule. At the same time, we find that the energy required for dissociating one in four water molecules, so as to obtain the model interface shown in Fig. 3, is only 60 meV. This surprisingly small energy penalty results from the balance between the cost of splitting H_2O and the energy gained by forming the H bond in the $\text{HO}\cdots\text{H}_2\text{O}$ complex discussed above. This result is similar to the case of water adsorption on rutile TiO_2 , where computational and experimental studies provide evidence for such complexes [9,11]. We find a similar trend for the case of an isolated water dimer. In this latter case, we calculate the energy required to form the $\text{HO}\cdots\text{H}_2\text{O}$ complex to be 150 meV; i.e., at very low coverage, complex-assisted dissociation is only slightly less favorable than at full coverage.

Given that the calculated total energies of the undissociated and of the partially dissociated monolayers differ by only 60 meV, we proceed with an analysis of quantum nuclear zero-point effects. For this purpose, we investigate the vibrational eigenmodes for two model surfaces, with H_2O adsorbed either molecularly or dissociatively. We find that upon dissociation the zero-point energy decreases by 80 meV. This decrease can be understood by noting that the contribution to the vibrational energy from the bending mode of the H_2O molecule at 1580 cm^{-1} is removed upon dissociation. After taking this zero-point correction into account, the partially (25%) dissociated water monolayer becomes marginally more stable (20 meV) than the molecular monolayer. Similarly, at low coverage the formation of the H complex is only marginally unstable (by 70 meV) and could be temperature activated. The above suggests that vibrational spectroscopy could be employed to quantify the fraction of dissociated water, through the relative intensities of the bending mode at 1580 cm^{-1} (present only for molecular H_2O) and the stretching modes at 3700 cm^{-1} (present for both molecular and dissociated H_2O).

Obviously, the energetic differences here are so small that these results may be sensitive to the choice of the

exchange and correlation functional and may be affected by the neglect of dispersion forces, subsurface defects, and step edges [37–40]. To demonstrate this aspect, we repeat full structural relaxations of the interface models using the PBE0 hybrid functional [30] which previously was shown to improve the accuracy of calculations of the vibrational properties of liquid water [41]. Interestingly, the formation energy of the $\text{HO}\cdots\text{H}_2\text{O}$ complex starting from two water molecules is reduced when using the PBE0 hybrid functional (Appendix A 5), further demonstrating that this complex plays an important role in the structure of water on TiO_2 .

Our present analysis of the adsorption energetics indicates that there may not necessarily be a contradiction between the spectroscopic observation of dissociated water and DFT calculations of adsorption energies. Previous calculations taken as evidence against dissociative adsorption, although technically correct, did not consider the possibility of forming the energetically favorable $\text{HO}\cdots\text{H}_2\text{O}$ complex, thus reaching conclusions that water adsorbs molecularly. Our calculations indicate that complex-assisted dissociation is slightly more favorable than molecular adsorption.

Having identified that the $\text{HO}\cdots\text{H}_2\text{O}$ complex might play an important role in the adsorption of water on anatase $\text{TiO}_2(101)$, we wanted to check whether this complex might be related to the 2×2 superstructure observed in the STM experiments of Ref. [20] at high coverage. To this aim, we calculated the STM map of a monolayer of the $\text{HO}\cdots\text{H}_2\text{O}$ complex in the Tersoff-Hamann approximation [42] (Fig. 4). Our choice of performing the calculation for a full monolayer is dictated by computational convenience and does not affect our analysis, since the STM map is effectively a local density of states [42].

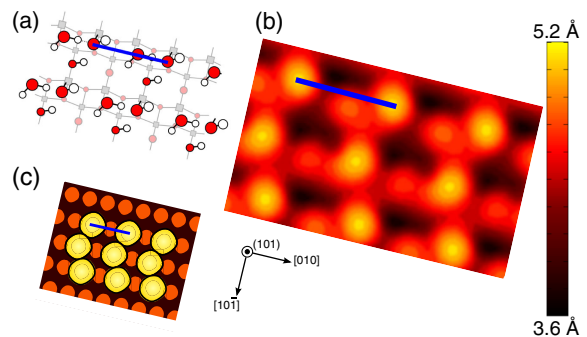


FIG. 4. Ball-and-stick representation (a) and calculated STM map (b) for a monolayer of $\text{HO}\cdots\text{H}_2\text{O}$ complexes. A cartoon sketch to scale of the images reported in Ref. [20] featuring the experimentally measured topography is shown in (c). The STM map was calculated [42] as an isovalue plot (3.0×10^{-4} electrons \AA^{-3}) of the local density of states integrated over an energy window of 2.1 eV above the conduction band edge of TiO_2 . The blue segment is along the [010] direction and measures 7.6 \AA . The elevation is given with respect to the fivefold-coordinated Ti sublattice.

The calculated STM map consists of bright spots aligned along the [010] direction, derived from the empty O $2p$ states of the OH groups. Interestingly, we found that our calculated maps are in agreement with the topography measured in Ref. [20], accounting for the doubling of the period along the [010] direction. Reproducing this period doubling with exclusively molecular water requires that H₂O molecules do not adsorb on adjacent sites [20] (cf. Appendix A 6). A partially dissociated monolayer with a significant fraction of HO \cdots H₂O complexes provides an alternative explanation of the measured STM images. Additional discussion of experimental studies of the anatase TiO₂:H₂O interface is provided in Appendix B.

IV. CONCLUSIONS

In summary, our first-principles calculations support the assignment of dissociated water in the XPS experiments of Ref. [21] on the TiO₂ anatase (101) surface at monolayer coverage. In this configuration, water dissociation is enabled by the H-bonded complex HO \cdots H₂O. We demonstrate that this complex is energetically more favorable than molecular adsorption and that it can provide an alternative explanation for the 2×2 superstructure observed in the STM images of Ref. [20]. Taken together, our present findings outline a structural model of the TiO₂:H₂O interface which is compatible with a variety of experimental and theoretical studies on this important photocatalytic interface. More generally, this work demonstrates how the reverse engineering of experimental data using *ab initio* spectroscopy represents a powerful tool for elucidating the nature of complex materials for energy applications.

ACKNOWLEDGMENTS

This work was supported by the European Research Council (EU FP7/ERC Grant No. 239578), the United Kingdom Engineering and Physical Sciences Research Council (Grant No. EP/J009857/1), and the Leverhulme Trust (Grant No. RL-2012-001). Calculations were performed at the Oxford Supercomputing Centre and at the Oxford Materials Modelling Laboratory. Figures were rendered by using VMD [43].

APPENDIX A: COMPUTATIONAL DETAILS

1. DFT calculations

The plane-wave kinetic energy cutoffs of wave functions and charge density are 35 and 200 Ry, respectively. The core-valence interaction is treated by means of ultrasoft pseudopotentials [26], with the semicore Ti $3s$ and $3p$ states explicitly described. The TiO₂ substrate is modeled as a stoichiometric slab, obtained by cutting bulk anatase along the (101) plane [14,22]. The resulting slab consists of eight TiO₂ layers (12.9-Å thickness), with the periodic slab

replicas separated by a vacuum region of 15 Å. The minimal surface cell considered here has dimensions 10.4×7.6 Å² and contains four TiO₂ units. For the calculation of interface geometries, adsorption energies, and STM maps, we sample the surface Brillouin zone by using a 2×2 grid, while for calculations of core-level shifts we use a 2×2 supercell (monolayer coverage) and a 1×2 supercell (low coverage), both with Γ -point sampling. Calculations using the 2×2 surface supercell (432 atoms) are necessary in order to minimize the interaction of charged replicas [24,27]. Geometry optimizations are performed with the bottom TiO₂ layer fixed in order to mimic a semi-infinite substrate and carried out until the forces on all the other atoms are below 30 meV/Å. The vibrational eigenmodes and eigenfrequencies for the calculation of zero-point energies are obtained within the harmonic approximation, by using the method of finite displacements [28] and the minimal surface unit cell.

2. Sensitivity to electron escape depth

Throughout our study, we use a value of 3.5 Å for the electron escape depth λ , which is physically reasonable based on the energies of the incident x rays and electron binding energies [33]. In Fig. 5, we illustrate the effect of using different values for λ . It can be seen that the escape depth essentially determines the relative strength of the bulk and adsorbate contributions to the spectrum. Intuitively, larger values of λ reduce the surface sensitivity. We find that the structure of the adsorbate contribution at 532 eV and above is insensitive to λ . This observation can be rationalized by noting that the oxygen atoms of molecular and dissociated H₂O are located at similar distances from the surface. Comparing to the experimental data of Ref. [21] in Fig. 5(b) shows how choosing different values of λ cannot remedy the failure of the purely molecular monolayer to account for the experimentally observed features.

3. Dissociative adsorption of H₂O at low coverage

In dissociative adsorption of H₂O, the OH group binds covalently to a fivefold Ti atom (bond length 1.82 Å), and the remaining proton binds to a twofold O atom, thereby yielding an additional hydroxyl group. For completeness we explore models differing in the separation between these two OH groups (Fig. 6). The model with the additional hydroxyl group at the site labeled by L1 in Fig. 6 has previously been denoted the intrapair configuration [15] or pseudodissociated water [21]. The model with the additional OH group at site L2 was denoted the “interpair configuration” [15]. In accordance with the findings of Ref. [15], we find the intrapair configuration (L1) to be more stable than interpair (L2), by 0.05 eV per H₂O molecule. Configuration L3 is taken to describe the limit of isolated OH groups. Note that the description of L3 requires the use of a 1×2 supercell.

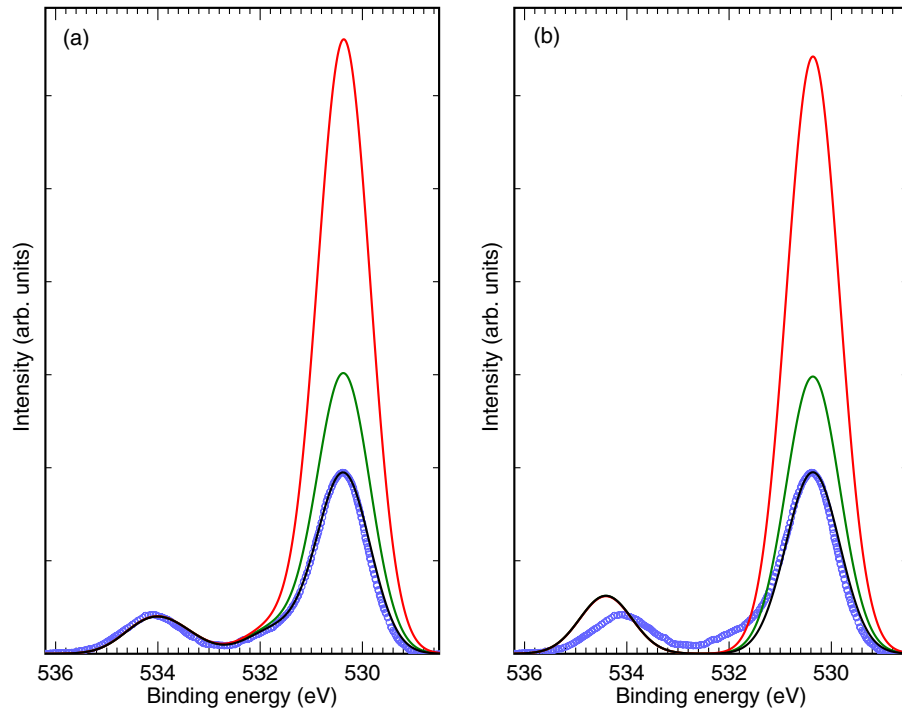


FIG. 5. Calculated O $1s$ core-level spectra for the $\text{TiO}_2:\text{H}_2\text{O}$ interface at monolayer coverage in the case of 25% H_2O dissociation (a) and fully molecular adsorption (b) for different values of the electron escape depth λ . The black, green, and red lines correspond to $\lambda = 3.5, 5.0,$ and 10.0 \AA , respectively. The experimental O $1s$ spectrum (blue circles, spectrum at 230 K in Fig. 3 of Ref. [21]) is also shown.

When calculating the O $1s$ spectrum for models L1–L3, in each case there are two new contributions to the spectrum from the inequivalent OH groups. As discussed in the main text, for L1 these contributions appear at 531.34 and 531.93 eV. Similarly, for configurations L2 and L3 the binding energies of the corresponding O atoms are 531.21 or 532.05 eV and 531.06 or 532.11 eV, respectively. These small differences are completely washed out when vibrational broadening is included. In fact, Fig. 6 shows that the

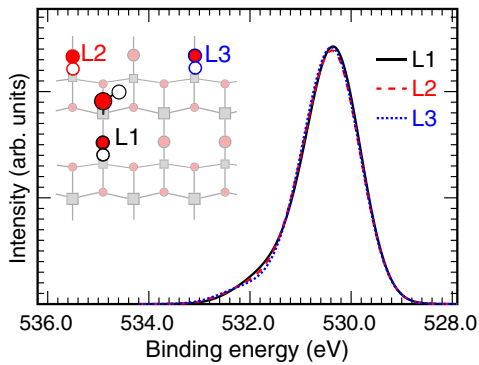


FIG. 6. Calculated O $1s$ core-level spectra for the $\text{TiO}_2:\text{H}_2\text{O}$ interface at low coverage in the case of dissociative adsorption, with the OH groups located at the different sites marked L1, L2, and L3. The spectra (shown as solid, red dashed, and blue dotted curves, respectively) were calculated with a Gaussian broadening of 1.2 eV and are practically indistinguishable.

spectra of the various configurations of dissociated water at low coverage are practically indistinguishable. This finding indicates that hydroxyl-hydroxyl interactions can safely be neglected in the interpretation of O $1s$ core-level spectra.

4. Numerical convergence of adsorption energies

Since the presence of dissociated water on the anatase $\text{TiO}_2(101)$ surface is at variance with the commonly accepted molecular model of the $\text{TiO}_2:\text{H}_2\text{O}$ interface [15,16,19,20], we reexamined the adsorption energetics. In this section, we focus on numerical convergence.

Figure 7 displays the adsorption energies of isolated molecular and dissociated H_2O on the anatase $\text{TiO}_2(101)$ surface, calculated as a function of the surface Brillouin zone (k -point) sampling or TiO_2 slab thickness. Using Γ -point sampling and a slab of four TiO_2 layers (the same computational setup as Ref. [15]), we calculate adsorption energies of 0.70 and 0.32 eV for molecular and dissociated water, respectively (difference 0.38 eV). Keeping the slab thickness fixed at four TiO_2 layers but increasing the Brillouin zone sampling to 2×2 (left plot of Fig. 7) causes small changes in the adsorption energies, to 0.67 and 0.33 eV (difference 0.34 eV); further increasing the sampling to 3×3 results in changes of less than 0.005 eV to the adsorption energies. Thus, we see that the difference between molecular and dissociative adsorption energies reduces by 0.04 eV upon converging with k points.

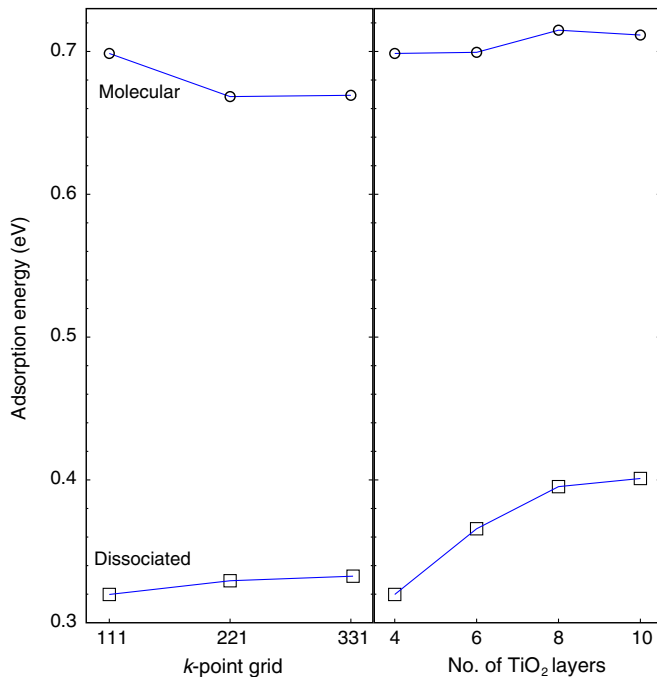


FIG. 7. Convergence of the adsorption energies for molecular (circles) and dissociative (squares) H_2O adsorption as a function of k -point sampling and thickness of the TiO_2 slab. For dissociative adsorption, the intrapair configuration (L1 in Fig. 6) is considered. In the test of convergence with k points a slab of four TiO_2 layers is used, while in the test of convergence with slab thickness Γ -point sampling is used. All other computational details are as reported in Appendix A 1. The blue lines are guides to the eye.

Now fixing the Brillouin zone sampling to the Γ point and instead varying the slab thickness (right plot of Fig. 7), we observe differing convergence behavior for molecular and dissociative adsorption. Upon increasing the slab thickness through the sequence $4 \rightarrow 6 \rightarrow 8 \rightarrow 10$ layers, the molecular adsorption energy takes the values $0.70 \rightarrow 0.70 \rightarrow 0.71 \rightarrow 0.71$ eV, i.e., a change of 0.01 eV on tripling the thickness of the slab (5.8–16.4 Å). Meanwhile, the variation in adsorption energy for dissociative H_2O is an order of magnitude larger, taking the values $0.32 \rightarrow 0.37 \rightarrow 0.40 \rightarrow 0.40$ eV. Thus, the difference between molecular and dissociative adsorption energies decreases from 0.38 to 0.31 eV after converging the results with the thickness of the TiO_2 slab.

Our convergence tests reveal that increasing either k -point sampling or slab thickness reduces the difference in molecular and dissociative adsorption energies. Converging both quantities together further reduces this difference. Using a 2×2 k -point sampling and an eight-layer TiO_2 slab, we obtain adsorption energies of 0.69 and 0.42 eV for molecular and dissociative H_2O , respectively. The obtained difference in adsorption energies, 0.27 eV, is 0.11 eV smaller than the unconverged case. As a footnote, we note that our calculations highlight a potential danger

with using only the molecular adsorption energy to test convergence, since this quantity changes by less than 0.001 eV on moving from a four- to a six-layer slab.

5. Hybrid functional calculations of adsorption energetics

Our work has shown that careful numerical convergence, combined with consideration of quantum nuclear zero-point effects, leads to energetic differences between molecular and partially dissociated models of the $\text{TiO}_2:\text{H}_2\text{O}$ interface which are very small; at monolayer coverage the partially dissociated monolayer is favorable by 20 meV, while at low coverage the cost of forming the H-bonded $\text{HO} \cdots \text{H}_2\text{O}$ complex is found to be 70 meV. These energy differences are so small that the results may be sensitive to the choice of the exchange and correlation functional. To explore this point further, we decide to repeat our calculations of adsorption geometries and energies by using the PBE0 hybrid functional [30], which has previously been shown to improve the accuracy of calculations of the vibrational properties of liquid water [41].

A difficulty with hybrid functional approaches, particularly when combined with plane-wave basis sets, is their significant computational expense as compared to local or semilocal functionals. Furthermore, the implementation of hybrid functional calculations in the current general release of QUANTUM ESPRESSO is not compatible with ultrasoft pseudopotentials. Therefore, we employ a reduced computational setup for the hybrid functional calculations and use norm-conserving pseudopotentials. In order that we might assess the effect of the exact exchange directly, we also perform additional calculations with an identical computational setup at the PBE level of theory. Finally, we compare the values calculated within the reduced computational setup with the fully converged PBE values, calculated as described in Appendix A 1.

The reduced computational setup is described as follows. The core-valence interaction is treated by means of norm-conserving pseudopotentials, with the Ti $3s$ and $3p$ states frozen into the core. A converged value of 100 Ry is used for the plane-wave kinetic energy cutoff of the wave functions. A 1×1 surface cell is used to construct structural models, as for the fully converged setup; however, the slab thickness is reduced to four TiO_2 layers and the Brillouin zone sampled at the Γ point only. The lattice parameters used to construct the slab are obtained by relaxing anatase TiO_2 in bulk with the norm-conserving pseudopotentials at the PBE level of theory, sampling the Brillouin zone on a $6 \times 6 \times 6$ mesh. The periodic slab replicas are separated by a vacuum region of 9 Å. Full geometry optimizations are performed exactly as in the fully converged setup, with the bottom TiO_2 layer fixed in order to mimic a semi-infinite layer and carried out until the forces on all the other atoms are below 30 meV/Å.

The structural models considered at the PBE0 level of theory are shown in Fig. 8. We obtain the fully relaxed geometries of (a) molecularly adsorbed H_2O at low coverage, (b) dissociated (intrapair) H_2O at low coverage, (c) two molecularly adsorbed H_2O molecules, and (d) the H-bonded $\text{HO}\cdots\text{H}_2\text{O}$ complex. We also obtain the structure of the clean anatase $\text{TiO}_2(101)$ slab and of the isolated H_2O molecule.

Table I gives the adsorption energies calculated with the reduced computational setup using either the PBE or PBE0 functional to account for exchange and correlation. For comparison, we also provide the same quantities calculated with the PBE functional and the fully converged computational setup. The table shows the adsorption energies calculated for molecular and dissociated water, and their difference, and also gives the energy cost of forming the $\text{HO}\cdots\text{H}_2\text{O}$ complex. The latter is obtained as a total energy difference between the models shown in Figs. 8(c) and 8(d). The data of the last two columns of Table I are displayed as bar charts in Figs. 8(e) and 8(f).

Our hybrid functional calculations produce some interesting results. First, comparing the energies for molecular and dissociative adsorption at the reduced computational setup, we find that the PBE0 hybrid functional predicts an increased stability of dissociative adsorption compared to PBE. Overall, the difference in molecular and dissociative adsorption energies decreases by 0.10 eV in the PBE0 calculations [Fig. 8(e)]. Further comparing the PBE calculations obtained for the reduced and converged computational setups, we find this same difference to decrease by

TABLE I. Adsorption energetics calculated with the reduced computational setup at the PBE or PBE0 level of theory or at the PBE level of theory at the converged (conv.) computational setup. The corresponding models of molecular and dissociated H_2O on the anatase $\text{TiO}_2(101)$ surface are shown in Figs. 8(a) and 8(b). The table also gives the difference in molecular and dissociated adsorption energies and the energy cost of forming the H-bonded $\text{HO}\cdots\text{H}_2\text{O}$ complex from two molecularly adsorbed H_2O molecules [Figs. 8(c) and 8(d)]. The data of the last two columns are displayed as bar charts in Figs. 8(e) and 8(f). All values are in eV.

	Molecular	Dissociated	Difference	Complex
PBE	0.80	0.42	0.38	0.41
PBE0	0.84	0.56	0.28	0.27
PBE (conv.)	0.69	0.42	0.27	0.15

0.11 eV. Therefore, we expect that the calculated difference between molecular and dissociative H_2O adsorption with PBE0 of 0.28 eV represents an upper bound, and further converging these calculations with k points and slab thickness would further reduce this difference.

Second, considering the energy cost of forming the complex [Fig. 8(f)], we again find a reduction on moving to the PBE0 level of theory, by 0.14 eV. This reduction can be attributed to the lower cost of water dissociation in PBE0 (0.10 eV, as discussed above) and to a stronger hydrogen bond in the $\text{HO}\cdots\text{H}_2\text{O}$ complex (0.04 eV). Again noting that the energy cost of forming the complex decreases by 0.26 eV on moving from the reduced to the converged computational setups at the PBE level of theory, we are left

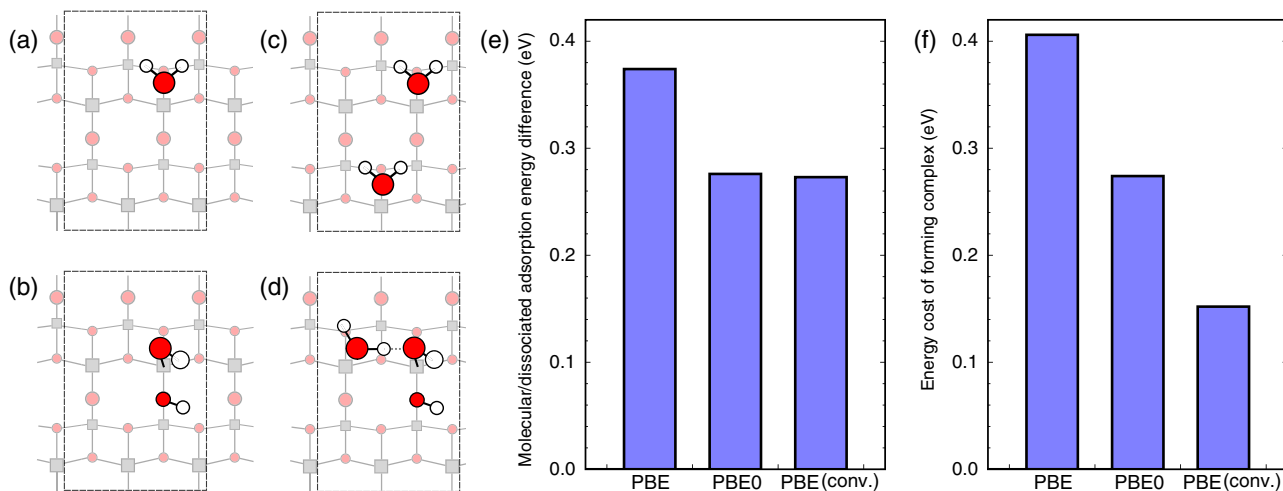


FIG. 8. (a)–(d) Ball-and-stick representations of H_2O adsorption models used to test the effect of including exact exchange into calculations of adsorption energies, corresponding to (a) molecular adsorption, (b) dissociated adsorption, (c) two molecularly adsorbed H_2O molecules per unit cell, and (d) the H-bonded $\text{HO}\cdots\text{H}_2\text{O}$ complex. The dashed-line rectangles show the surface unit cell. (e),(f) Bar charts giving adsorption energies calculated by using different approaches. The labels “PBE” and “PBE0” denote the exchange-correlation functionals used to calculate adsorption energies within the reduced computational setup. “PBE (conv.)” refers to calculations performed with the converged computational setup described in Appendix A 1 and used throughout our study. The bars shown in (e) give the difference in molecular and dissociative adsorption energies, obtained as the total energy difference between the models shown in (a) and (b). The bars shown in (f) give the energy cost of forming the $\text{HO}\cdots\text{H}_2\text{O}$ complex, obtained as the total energy difference between the models shown in (c) and (d).

with a possibility that a fully converged PBE0 calculation would predict the $\text{HO}\cdots\text{H}_2\text{O}$ complex to be stable even before considering the vibrational contribution to the energy.

As well as adsorption energetics, the full geometry relaxations provide insight into the different descriptions of the structure of the H-bonded $\text{HO}\cdots\text{H}_2\text{O}$ complex in PBE and PBE0. We found that the length of the H bond [dotted line in Fig. 8(d)] increases by just 0.012 Å on moving from PBE to PBE0. This observation can be explained simply by noting that the formation of the $\text{HO}\cdots\text{H}_2\text{O}$ complex is determined by the competition of the covalent Ti—O bond of the hydroxyl, the covalent Ti—O bond of the H_2O molecule, and the H bond between the hydroxyl and H_2O molecule. Given the enhanced strength of covalent bonds compared to H bonds, it is not surprising that there are fewer changes observed on moving from a semilocal to nonlocal description of exchange compared to that observed for homogeneous molecular water [41], where H bonds dominate.

Clearly, in light of the discussion of numerical convergence in the previous section, the values presented in Table I and Figs. 8(e) and 8(f) cannot be considered definitive. However, the hybrid functional calculations clearly show that the energetic balance between molecular and dissociative H_2O adsorption on the anatase $\text{TiO}_2(101)$ surface is extremely delicate. As a consequence, we conclude that current first-principles calculations cannot rule out the possibility of water dissociation on this surface.

6. STM image of the molecular monolayer

Figure 9 shows the calculated STM image of purely molecularly adsorbed water. Each adsorbed water molecule appears as a bright spot in the spectrum, with the calculated image thus showing a 1×1 periodicity. In order to account for the experimentally observed 2×2 periodicity using only molecular water, it is necessary for water not to adsorb at adjacent sites but rather be staggered, as proposed in Ref. [20].

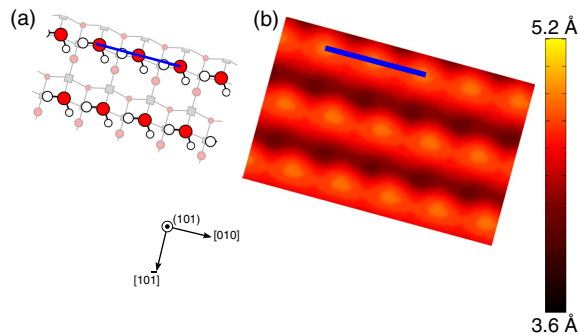


FIG. 9. Ball-and-stick model (a) and calculated STM image (b) of purely molecularly adsorbed water. The STM image is obtained by using the same computational setup as in Fig. 4 of the main text. As in Fig. 4, the blue segment measures 7.6 Å.

APPENDIX B: EXPERIMENTAL STUDIES OF WATER ADSORPTION AT THE ANATASE $\text{TiO}_2:\text{H}_2\text{O}$ INTERFACE

In 1998, the authors of Ref. [15] considered previous experimental studies of the anatase $\text{TiO}_2:\text{H}_2\text{O}$ interface and noted: “On the basis of this experimental information, different models of the anatase surface and of water adsorption at this surface have been proposed, but no clear picture has emerged yet.” Subsequently, to our knowledge three experimental works were published aimed at obtaining a clearer picture of the behavior of water on well-defined anatase (101) surfaces: a combined temperature-programmed desorption and XPS study [16], an STM study [20], and another XPS study published more recently [21].

Our current work supports the interpretation of the XPS measurements of Ref. [21] as evidence for water dissociation. We also show that features found in the STM images measured in Ref. [20] (the 2×2 superstructure and zigzag pattern) can also be explained in terms of a partially dissociated monolayer of H_2O , although the authors of Ref. [20] provide an alternative explanation in terms of a purely molecular monolayer.

The remaining experimental work is the TPD and XPS study of Ref. [16]. First considering the XPS, comparing the measurements of Ref. [16] to Ref. [21] shows that the latter has achieved the higher resolution in measuring the $\text{O } 1s$ spectrum. This higher resolution is essential to discern the presence of OH groups, since they appear only as a shoulder to the bulk TiO_2 peak [cf. Fig. 2(b) of our work]. Partial dissociation of H_2O stabilized by H-bonding interactions also provides an explanation for the coverage-dependent shift of the molecular H_2O peak observed in Ref. [16], since our calculations showed that this feature is sensitive to intermolecular H bonding.

Now turning to the TPD measurements, the TPD spectrum of hydrated anatase shows a broad peak at 250 K and additional features at 190 and 160 K at coverages greater than one monolayer. In contrast to experiments performed on the rutile (110) surface [44], there is no peak at approximately 500 K. The absence of this peak was considered significant, since the 500-K feature in rutile was assigned to dissociated water in Ref. [44]. However, as noted by the authors of Ref. [16], the hydroxyls found on the rutile (110) surface are thought to form at O vacancies; therefore, it is not clear how the behavior of hydroxyl species formed at defects on rutile should correspond to that of dissociated water on the stoichiometric anatase surface. Indeed, we note that the calculations of Ref. [45] found an adsorption energy of 0.94 eV for dissociated H_2O on the defective rutile (110) surface, which is larger than the adsorption energies calculated for water on stoichiometric anatase. In fact, as shown by the XPS measurements at different temperatures reported in Ref. [21], the hydroxyl groups on the anatase

(101) surface observed by the XPS have all been desorbed by 400 K.

The question remains, therefore, of how to assign the broad peak observed in the TPD spectrum at 250 K. The authors of Ref. [16] assign the peak as originating from the desorption molecular water only, on the basis that the adsorption energy obtained by them through a Redhead analysis was found to be similar to that obtained in the previous theoretical work of Ref. [15]. However, if the adsorption energies of molecular and dissociated H₂O are similar, as shown by our work, the broad peak at 250 K could equally be assigned to the desorption of both molecular and dissociated H₂O.

-
- [1] Y. Tachibana, L. Vayssieres, and J. R. Durrant, Artificial photosynthesis for solar water-splitting, *Nat. Photonics* **6**, 511 (2012).
- [2] A. Fujishima and K. Honda, Electrochemical photolysis of water at a semiconductor electrode, *Nature (London)* **238**, 37 (1972).
- [3] M. Grätzel, Photoelectrochemical cells, *Nature (London)* **414**, 338 (2001).
- [4] Y. Paz, Z. Luo, L. Rabenberg, and A. Heller, Photooxidative self-cleaning transparent titanium dioxide films on glass, *J. Mater. Res.* **10**, 2842 (1995).
- [5] S. C. Roy, O. K. Varghese, M. Paulose, and C. A. Grimes, Toward solar fuels: Photocatalytic conversion of carbon dioxide to hydrocarbons, *ACS Nano* **4**, 1259 (2010).
- [6] H. H. Kristoffersen, J. O. Hansen, U. Martinez, Y. Y. Wei, J. Matthiesen, R. Streber, R. Bechstein, E. Lægsgaard, F. Besenbacher, B. Hammer, and S. Wendt, Role of steps in the dissociative adsorption of water on rutile TiO₂(110), *Phys. Rev. Lett.* **110**, 146101 (2013).
- [7] L.-M. Liu, C. Zhang, G. Thornton, and A. Michaelides, Structure and dynamics of liquid water on rutile TiO₂(110), *Phys. Rev. B* **82**, 161415 (2010).
- [8] F. Allegretti, S. O'Brien, M. Polcik, D. I. Sayago, and D. P. Woodruff, Adsorption bond length for H₂O on TiO₂(110): A key parameter for theoretical understanding, *Phys. Rev. Lett.* **95**, 226104 (2005).
- [9] J. Matthiesen, J. Ø. Hansen, S. Wendt, E. Lira, R. Schaub, E. Lægsgaard, F. Besenbacher, and B. Hammer, Formation and diffusion of water dimers on rutile TiO₂, *Phys. Rev. Lett.* **102**, 226101 (2009).
- [10] I. M. Brookes, C. A. Muryn, and G. Thornton, Imaging water dissociation on TiO₂(110), *Phys. Rev. Lett.* **87**, 266103 (2001).
- [11] P. J. D. Lindan, and C. Zhang, Exothermic water dissociation on the rutile TiO₂(110) surface, *Phys. Rev. B* **72**, 075439 (2005).
- [12] U. Diebold, The surface science of titanium dioxide, *Surf. Sci. Rep.* **48**, 53 (2003).
- [13] V. Shklover, Y. E. Ovchinnikov, L. S. Braginsky, S. M. Zakeeruddin, and M. Grätzel, Structure of organic/inorganic interface in assembled materials comprising molecular components. Crystal structure of the sensitizer bis[(4,4-carboxy-2,2-bipyridine)(thiocyanato)]ruthenium(II), *Chem. Mater.* **10**, 2533 (1998).
- [14] M. Lazzeri, A. Vittadini, and A. Selloni, Structure and energetics of stoichiometric TiO₂ anatase surfaces, *Phys. Rev. B* **63**, 155409 (2001).
- [15] A. Vittadini, A. Selloni, F. P. Rotzinger, and M. Grätzel, Structure and energetics of water adsorbed at TiO₂ anatase (101) and (001) surfaces, *Phys. Rev. Lett.* **81**, 2954 (1998).
- [16] G. S. Herman, Z. Dohnálek, N. Ruzycski, and U. Diebold, Experimental investigation of the interaction of water and methanol with anatase TiO₂(101), *J. Phys. Chem. B* **107**, 2788 (2003).
- [17] M. Raju, S.-Y. Kim, A. C. van Duin, and K. A. Fichthorn, ReaxFF reactive force field study of the dissociation of water on titania surfaces, *J. Phys. Chem. C* **117**, 10558 (2013).
- [18] C. Arrouvel, M. Digne, M. Breyse, H. Toulhoat, and P. Raybaud, Effects of morphology on surface hydroxyl concentration: A DFT comparison of anatase TiO₂ and γ -alumina catalytic supports, *J. Catal.* **222**, 152 (2004).
- [19] C. Sun, L.-M. Liu, A. Selloni, G. Q. Lu, and S. C. Smith, Titania-water interactions: A review of theoretical studies, *J. Mater. Chem.* **20**, 10319 (2010).
- [20] Y. He, A. Tilocca, O. Dulub, A. Selloni, and U. Diebold, Local ordering and electronic signatures of submonolayer water on anatase TiO₂(101), *Nat. Mater.* **8**, 585 (2009).
- [21] L. E. Walle, A. Borg, E. M. J. Johansson, S. Plogmaker, H. Rensmo, P. Uvdal, and A. Sandell, Mixed dissociative and molecular water adsorption on anatase TiO₂(101), *J. Phys. Chem. C* **115**, 9545 (2011).
- [22] C. E. Patrick and F. Giustino, O 1s core-level shifts at the anatase TiO₂(101)/N₃ photovoltaic interface: Signature of H-bonded supramolecular assembly, *Phys. Rev. B* **84**, 085330 (2011).
- [23] M. Pozzo, D. Alfè, P. Lacovig, P. Hofmann, S. Lizzit, and A. Baraldi, Thermal expansion of supported and freestanding graphene: Lattice constant versus interatomic distance, *Phys. Rev. Lett.* **106**, 135501 (2011).
- [24] J. F. Binder, P. Broqvist, H.-P. Komsa, and A. Pasquarello, Germanium core-level shifts at Ge/GeO₂ interfaces through hybrid functionals, *Phys. Rev. B* **85**, 245305 (2012).
- [25] J. P. Perdew, K. Burke, and M. Ernzerhof, Generalized gradient approximation made simple, *Phys. Rev. Lett.* **77**, 3865 (1996).
- [26] D. Vanderbilt, Soft self-consistent pseudopotentials in a generalized eigenvalue formalism, *Phys. Rev. B* **41**, 7892 (1990).
- [27] G. Makov and M. C. Payne, Periodic boundary conditions in ab initio calculations, *Phys. Rev. B* **51**, 4014 (1995).
- [28] G. J. Ackland, M. C. Warren, and S. J. Clark, Practical methods in ab initio lattice dynamics, *J. Phys. Condens. Matter* **9**, 7861 (1997).
- [29] P. Giannozzi *et al.*, QUANTUM ESPRESSO: A modular and open-source software project for quantum simulations of materials, *J. Phys. Condens. Matter* **21**, 395502 (2009).
- [30] C. Adamo and V. Barone, Toward reliable density functional methods without adjustable parameters: The PBE0 model, *J. Chem. Phys.* **110**, 6158 (1999).
- [31] E. Pehlke and M. Scheffler, Evidence for site-sensitive screening of core holes at the Si and Ge (001) surface, *Phys. Rev. Lett.* **71**, 2338 (1993).

- [32] A. Pasquarello, M. S. Hybertsen, and R. Car, Theory of Si 2p core-level shifts at the Si(001)-SiO₂ interface, *Phys. Rev. B* **53**, 10942 (1996).
- [33] K. Shimada, in *Very High Resolution Photoelectron Spectroscopy*, edited by S. Hüfner (Springer, Berlin, 2007).
- [34] C. E. Patrick and F. Giustino, Quantum nuclear dynamics in the photophysics of diamondoids, *Nat. Commun.* **4**, 2006 (2013).
- [35] S. Garcia-Gil, A. Arnau, and A. Garcia-Lekue, Coordinated H-bonding between porphyrins on metal surfaces, *Surf. Sci.* **613**, 102 (2013).
- [36] K. Andersson, A. Nikitin, L. G. M. Pettersson, A. Nilsson, and H. Ogasawara, Water dissociation on Ru (001): An activated process, *Phys. Rev. Lett.* **93**, 196101 (2004).
- [37] M. J. Gillan, F. R. Manby, M. D. Towler, and D. Alfè, Assessing the accuracy of quantum Monte Carlo and density functional theory for energetics of small water clusters, *J. Chem. Phys.* **136**, 244105 (2012).
- [38] X. Ren, P. Rinke, C. Joas, and M. Scheffler, Random-phase approximation and its applications in computational chemistry and materials science, *J. Mater. Sci.* **47**, 7447 (2012).
- [39] U. Aschauer, Y. He, H. Cheng, S.-C. Li, U. Diebold, and A. Selloni, Influence of subsurface defects on the surface reactivity of TiO₂: Water on anatase (101), *J. Phys. Chem. C* **114**, 1278 (2010).
- [40] X.-Q. Gong, A. Selloni, M. Batzill, and U. Diebold, Steps on anatase TiO₂(101), *Nat. Mater.* **5**, 665 (2006).
- [41] C. Zhang, D. Donadio, F. Gygi, and G. Galli, First principles simulations of the infrared spectrum of liquid water using hybrid density functionals, *J. Chem. Theory Comput.* **7**, 1443 (2011).
- [42] J. Tersoff and D. R. Hamann, Theory of the scanning tunneling microscope, *Phys. Rev. B* **31**, 805 (1985).
- [43] W. Humphrey, A. Dalke, and K. Schulten, VMD—Visual molecular dynamics, *J. Mol. Graphics* **14**, 33 (1996).
- [44] D. D. Beck, J. M. White, and C. T. Ratcliffe, Catalytic reduction of carbon monoxide with hydrogen sulfide. 2. Adsorption of water and hydrogen sulfide on anatase and rutile, *J. Phys. Chem.* **90**, 3123 (1986).
- [45] R. Schaub, P. Thostrup, N. Lopez, E. Lægsgaard, I. Stensgaard, J. K. Nørskov, and F. Besenbacher, Oxygen vacancies as active sites for water dissociation on rutile TiO₂(110), *Phys. Rev. Lett.* **87**, 266104 (2001).